2009

Laser-driven soft-X-ray undulator source

Matthias Fuchs
University of Nebraska - Lincoln, mfuchs@unl.edu

Raphael Weingartner
Max-Planck-Institut für Quantenoptik

Antonia Popp
Max-Planck-Institut für Quantenoptik

Zsuzsanna Major
Max-Planck-Institut für Quantenoptik

Stefan Becker
Ludwig-Maximilians-Universität

See next page for additional authors

Published in *Nature Physics* 5 (2009), pp. 826–829; doi: 10.1038/nphys1404

Submitted June 9, 2009; accepted August 26, 2009; published online September 27, 2009.

Laser-driven soft-X-ray undulator source

Matthias Fuchs,[1,2] Raphael Weingartner,[1,2] Antonia Popp,[1] Zsuzsanna Major,[1,2] Stefan Becker,[2] Jens Osterhoff,[1,2] Isabella Cortrie,[2] Benno Zeitler,[2] Rainer Hörlein,[1,2] George D. Tsakiris,[1] Ulrich Schramm,[3] Tom P. Rowlands-Rees,[4] Simon M. Hooker,[4] Dietrich Habs,[1,2] Ferenc Krausz,[1,2] Stefan Karsch,[1,2] and Florian Grüner[1,2]

1. Max-Planck-Institut für Quantenoptik, Hans-Kopfermann-Str. 1, 85748 Garching, Germany
2. Department für Physik, Ludwig-Maximilians-Universität, Am Coulombwall 1, 85748 Garching, Germany
3. Forschungszentrum Dresden–Rossendorf, Bautzner Landstraße 128, 01328 Dresden, Germany
4. University of Oxford, Clarendon Laboratory, Parks Road, Oxford OX1 3PU, UK

Corresponding authors — Stefan Karsch, stefan.karsch@mpq.mpg.de ; Florian Grüner florian.gruener@physik.uni-muenchen.de

Abstract

Synchrotrons and free-electron lasers are the most powerful sources of X-ray radiation. They constitute invaluable tools for a broad range of research[1]; however, their dependence on large-scale radiofrequency electron accelerators means that only a few of these sources exist worldwide. Laser-driven plasma-wave accelerators[2–10] provide markedly increased accelerating fields and hence offer the potential to shrink the size and cost of these X-ray sources to the university-laboratory scale. Here, we demonstrate the generation of soft-X-ray undulator radiation with laser-plasma-accelerated electron beams. The well-collimated beams deliver soft-X-ray pulses with an expected pulse duration of ~10 fs (inferred from plasma-accelerator physics). Our source draws on a 30-cm-long undulator[11] and a 1.5-cm-long accelerator delivering stable electron beams[10] with energies of ~210 MeV. The spectrum of the generated undulator radiation typically consists of a main peak centred at a wavelength of ~18 nm (fundamental), a second peak near ~9 nm (second harmonic) and a high-energy cutoff at ~7 nm. Magnetic quadrupole lenses[11] ensure efficient electron-beam transport and demonstrate an enabling technology for reproducible generation of tunable undulator radiation. The source is scalable to shorter wavelengths by increasing the electron energy. Our results open the prospect of tunable, brilliant, ultrashort-pulsed X-ray sources for small-scale laboratories.

Resolving the structure and dynamics of matter on the atomic scale requires a probe with ångstrøm resolution in space and femtosecond to attosecond resolution in time. Third-generation synchrotron sources produce X-ray pulses with durations of typically a few tens of picoseconds and can achieve 100 fs by using complex beam-manipulation techniques[12, 13]. They have already proven their capability of imaging static structures with atomic (spatial) resolution[1] and upcoming X-ray free-electron lasers hold promise for also extending the temporal resolution into the atomic/sub-atomic range[14–18]. Both of these sources consist of an electron accelerator and an undulator, which is a periodic magnetic structure that forces the electrons to oscillate and emit radiation[19]. Whereas current facilities require a kilometer-scale accelerator, new laser-plasma accelerators offer the potential for a marked reduction in size and cost as well as pulse durations of a few femtoseconds.

Femtosecond-laser-driven plasma accelerators have produced quasi-monoenergetic electron beams[2–7] with energies up to 1 GeV (references 8, 9, 20, 21) from centimeter-scale interaction lengths. The concept is based on an ultra-intense laser pulse, which ionizes atoms of a gas target and excites a plasma wave. This trails the pulse at nearly the speed of light and generates longitudinal electric fields, which are more than three orders of magnitude larger than in conventional accelerators.[22] Plasma electrons can become trapped and accelerated in these fields to a well-defined ultra-relativistic energy, which is indicative of an electron bunch length confined to a fraction of the plasma wavelength (in our case ~15 μm). This intuitive picture is confirmed by particle-in-cell simulations, which have revealed characteristic bunch lengths of the order of 3 μm, corresponding to bunch durations of 10 fs (ref. 23).

Driving short-period undulators with these electron beams holds promise for brilliant ultrashort X-ray sources on a university-laboratory scale. So far, undulator radiation from laser-plasma-accelerated electrons has been reported only in the visible to infrared part of the electromagnetic spectrum.[24] Here, we demonstrate the reproducible generation of tunable, ultrashort undulator radiation in the soft-X-ray range by propagating electrons with energies of ~210 MeV through a specifically designed undulator with a period of 5 mm. The duration of this short-wavelength pulse is dominated by that of the electron bunch and hence estimated to be ~10 fs, about three orders of magnitude shorter than that of typical pulses produced by synchrotron sources[1] (for more details on electron-bunch duration and elongation during beam transport, see Supplementary Information). Detection of undulator radiation in some 70% of consecutive driver-laser shots indicates a remarkable reproducibility for a first proof-of-concept demonstration experiment. It can be attributed to a stable electron-acceleration scheme[10] and the use of magnetic lenses[11] to guide the electron beam through the undulator.

Undulators have a sinusoidal transverse magnetic field with an amplitude B_0 and period λ_u that define the deflection parameter[19] $K \propto B_0 \cdot \lambda_u$. In the rest frame of the relativistic electrons moving through this field, λ_u is contracted by the Lorentz factor γ, which is defined as the total electron energy E in units of the electron rest energy $m_o c^2$. The undulator field causes the electrons to oscillate transversely with an amplitude proportional to K, and as a result of this acceleration to emit radiation. In the laboratory frame, this emission occurs in a narrow cone in the forward direction. The measured wavelength is once more reduced by γ because of the Doppler shift, which varies with the detection angle θ. Taking into account the reduced longitudinal electron velocity caused by the transverse quivering motion, the detected wavelength for the nth harmonic is

$$\lambda = \frac{\lambda_u}{2n\gamma^2}\left(1 + \frac{K^2}{2} + \gamma^2\theta^2\right) \quad (1)$$

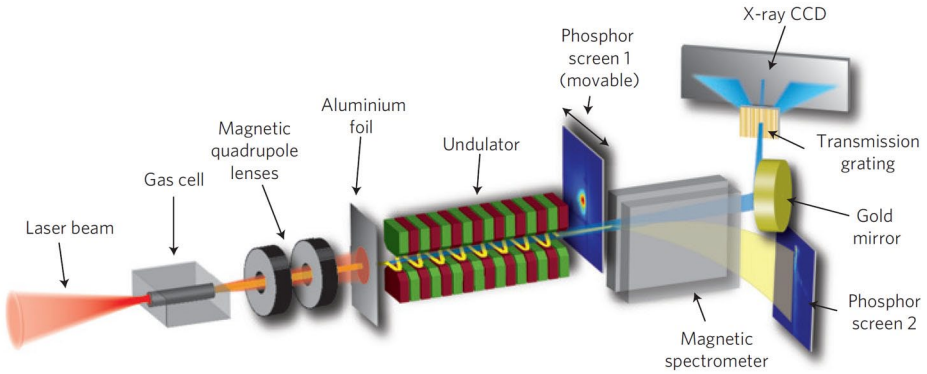

Figure 1. Experimental set-up. A laser pulse (red) is focused into a gas cell, in which plasma waves accelerate electrons (yellow) to energies of several hundred megaelectronvolts. The electron beam is collimated by a pair of quadrupole lenses. Plasma radiation and the laser beam are blocked by a 15 μm aluminum foil. The electrons propagate through an undulator and emit soft-X-ray radiation into a narrow cone along the forward direction (blue). The radiation is collected by a spherical gold mirror and characterized by a transmission grating in combination with an X-ray CCD camera. Stray light is blocked by a slit in front of the grating. The pointing, divergence and spectrum of the electron beam are diagnosed by phosphor screens.

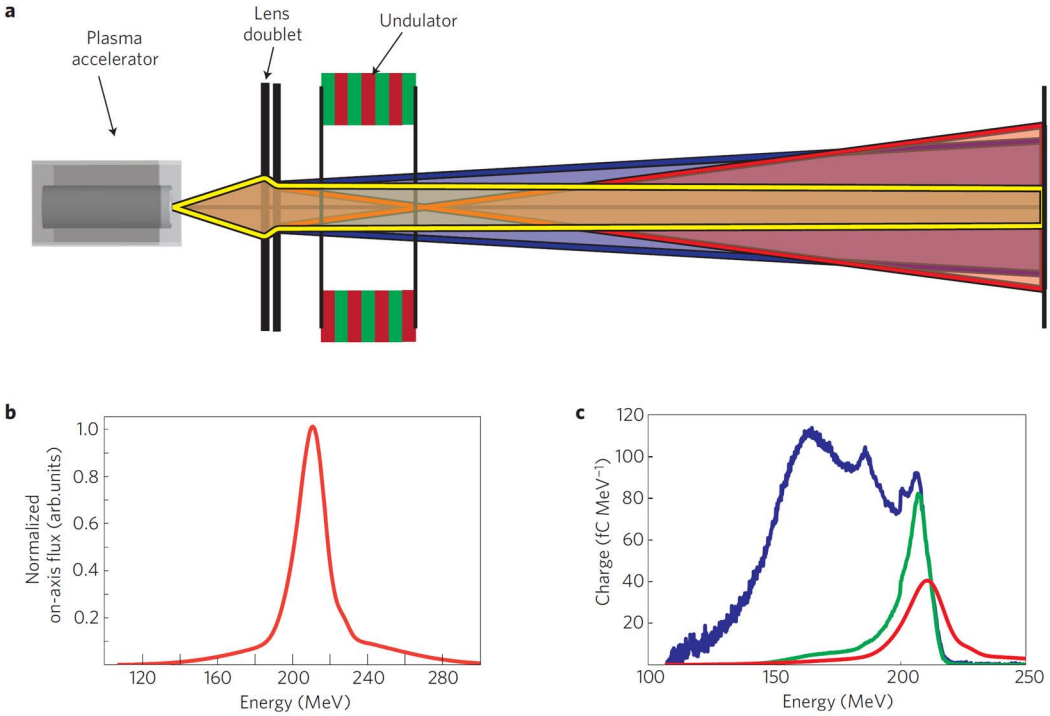

Figure 2. Effect of the magnetic lenses. a) Divergence of electrons traversing the magnetic lens assembly with energies of 190 MeV (red), 215 MeV (yellow) and 240 MeV (blue). **b)** Simulated normalized on-axis flux of the fundamental undulator emission versus electron energy ~260 cm downstream from the undulator exit (at the position of the detector). The narrow bandwidth of 9% FWHM is due to the energy-dependent electron-beam divergence introduced by the magnetic lenses. **c)** Measured electron spectrum (blue) corresponding to the undulator spectrum of Figure 3. The effective electron spectrum (green) is determined by the product of the measured spectrum (blue) and the system response curve (red in **b**,**c**). It has a bandwidth of 6% FWHM and a peak at 207 MeV.

In our experiment, the electron accelerator is driven by pulses from a 20 TW (850 mJ in 37 fs) laser system (see the Methods section). Focused into a hydrogen-filled gas cell with a length of 15 mm (Figure 1), they produce stable electron beams showing a quasi-monoenergetic energy spectrum with a stable peak in the range of 200–220 MeV and 7 pC of charge in the whole spectrum.

For electron-beam transport from the plasma accelerator to the undulator, we use a pair of miniature permanent-magnet quadrupole lenses, which has proven to be a critical system component for stable, reproducible operation of the undulator source for two reasons. First, they reduce the angular shot-to-shot fluctuations of the electron beam by an order of magnitude. Second, the lenses also act as an effective energy-band-pass filter for the undulator radiation and thus lower the photon-energy bandwidth and fluctuations. These benefits arise from the chromaticity of the lenses, which means that only electrons with a particular energy are collimated, whereas the divergence of electrons with different energies markedly increases (Figure 2a). As each individual electron emits its radiation in a narrow cone along its propagation direction, the whole photon beam has the approximate size and divergence of the emitting electron bunch. For that reason, it is possible to control the on-axis photon flux with the magnetic lenses by focusing the electron beam. In future applications, a small spot size on the target can therefore be achieved even for hard X-ray beams without the need for lossy optical focusing elements. For our set-up, a slightly convergent electron beam at ~210 MeV yields the highest on-axis photon flux at the detector, whereas deviations of a few tens of megaelectronvolts

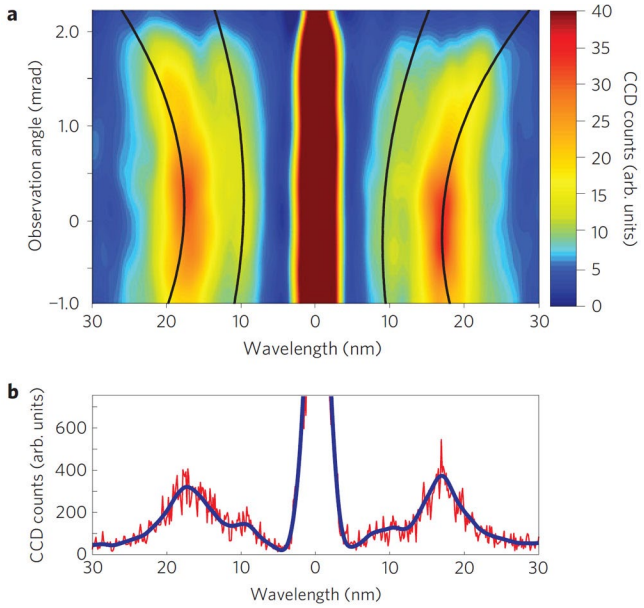

Figure 3. Single-shot spatially resolved undulator spectrum. **a)** Smoothed representation of the zeroth and the ± first diffraction order of the measured undulator spectrum corresponding to the electron spectrum of Figure 2c. It consists of a fundamental peak at 17 nm and a second harmonic peaked at 9 nm, with a high energy cutoff at ~7 nm. The theoretical parabolic dependence of the wavelength on the observation angle θ is shown by solid lines. An electron energy of 207 MeV corresponding to the peak of the effective electron spectrum of Figure 2c was used as a parameter. For the different emission characteristics of the second harmonic, our simulation yields an on-axis radiation spectrum peaked at a wavelength of 9.2 nm, which defines the parameter chosen for the corresponding parabola. **b)** On-axis lineout summed over 10 pixel rows around θ = 0 (blue) and the underlying raw data (red).

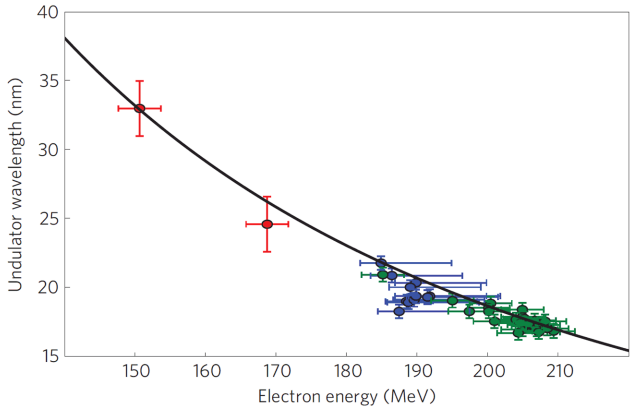

Figure 4. Undulator wavelength versus electron energy. Detected fundamental undulator radiation wavelengths plotted against the corresponding maxima of the effective electron spectra (determined by the method of Figure 2c). The green and blue points correspond to consecutive shots with two different positions of the magnetic lenses, demonstrating the wavelength-tunability of the source (see Supplementary Information). The error bars arise from measurement errors of the electron spectrometer, the X-ray spectrometer, magnetic lens distances and the undulator field. The asymmetric error bars of the blue points are due to a non-zero angle of the electron beam with the spectrometer axis. The red points represent shots that lie outside the stable electron acceleration regime. The theoretical behavior described in equation (1) is shown as a solid line.

cause this flux to drop sharply (Figure 2b). Thus, the magnetic lenses limit the energy range of electrons that primarily contribute to the undulator radiation and therefore define an "effective" electron spectrum (Figure 2c).

The influence of the electron-beam divergence on the angular flux of the undulator radiation at the position of the detector was computed with the code SRW (ref. 25), taking into account all beamline components (see the Methods section) to generate a "system response" curve (Figure 2b). An effective electron spectrum can be determined by multiplying this system response curve with the measured electron spectrum (shown in Figure 2c). This effective band-pass filtering reduces the shot-to-shot fluctuations of the spectral width and mean photon energy of the undulator emission as well as the bandwidth of an individual shot significantly below those of the corresponding electron spectra. For example, the fundamental spectrum of a single shot, shown in Figure 3, shows a bandwidth of 22% (full-width at half-maximum, FWHM) at an observation angle of θ = 0 (after deconvolving the instrument function deduced from the zeroth diffraction order), whereas a bandwidth of 65% would be expected without the filtering of the lenses. In 70% of consecutive laser shots we observed undulator spectra, whereas in the remaining 30% the amount of charge in the effective electron spectrum was insufficient to produce enough radiation. The average charge within the effective electron spectrum was 0.6 ± 0.3 pC, which produced 70,000 ± 25,000 photons in the undulator fundamental, integrated over a detection cone of $K/(2\gamma)$= ± 0.7 mrad, leading to a bandwidth of 30% FWHM. The observed spectra show a fundamental wavelength at 18 nm and a second harmonic peak at 10 nm with shot-to-shot standard deviations of about 5%.

The wavelength of the second harmonic is slightly longer than half the fundamental owing to its emission characteristics. In contrast to the fundamental, its flux distribution is peaked off-axis[19] ($\theta > 0$) with correspondingly longer wavelengths according to equation (1). Owing to the horizontally focusing mirror, these components are propagated through the slit onto the detector, shifting the peak of the observed on-axis spectrum to longer wavelengths.

Figure 3 shows the spectral and angular distribution of undulator radiation measured in a single shot. The parabolic dependence of the wavelength on the observation angle θ as predicted by equation (1) (see solid lines in Figure 3a), is in excellent agreement with the measured data. From the spectrum shown in Figure 3, we deduce (see the Methods section) that our source delivers 8,200 ± 3,100 photons per shot per mrad^2 per 0.1% bandwidth. An analytical estimation for the on-axis peak intensity in units of photons per shot per mrad^2 per 0.1% bandwidth for an undulator with a deflection parameter of K<1 is approximately given by[19] $N_{ph} \approx 1.744 \times 10^{14} N_u^2 \cdot E^2(\mathrm{GeV}) \cdot Q_e \cdot K^2/(1+K^2/2)$, where N_u is the number of undulator periods, E is the electron energy and Q_e is the charge of the electron bunch. According to this estimate, a charge of 1.3 pC in the effective electron spectrum (green curve in Figure 2c, which produced the undulator spectrum of Figure 3) corresponds to 9,500 ± 2,100 photons per shot per mrad^2 per 0.1% bandwidth. (The error is due to uncertainties in the calibration of the charge measurement and in the lens settings, both of which determine the amount of charge in the effective spectrum.) From the measured electron-beam divergence of ~1 mrad and source diameter of ~2 μm (derived from numerical simulations[23] and plausibility arguments involving the wakefield dimensions), we estimate the normalized electron-beam emittance as $\varepsilon_n = 0.8\pi$ mm mrad. For the central energy of the effective electron spectrum, this translates to a root-mean-square (r.m.s.) photon-beam size of 270 μm vertically and 630 μm horizontally in the undulator, with respective r.m.s. divergences of 180 and 170 μrad. Assuming a duration of 10 fs for the undulator radiation pulse, these estimates yield a peak brilliance of ~1.3 × 10^{17} photons per second per mrad^2 per mm^2 per 0.1% bandwidth.

Owing to the broad range of electron energies delivered by the plasma accelerator (blue curve in Figure 2c), the undulator source can be readily tuned to different wavelengths by changing the lens positions and thus shifting the system response (see Supplementary Figure S2) and effective electron spectrum shown (by the green curve) in Figure 2c. The correlation between the peak energy of the effective electron spectrum and the detected fundamental wavelength for different lens settings is shown in Figure 4. The dependence of wavelength on electron energy predicted by equation (1) is in excellent agreement with the measured data.

Our experiment paves the way for a new generation of brilliant, compact X-ray sources with the potential for widespread application in university-scale laboratories. Of key importance will be the few-femtosecond duration of emission inherent to laser-wakefield acceleration. This implies orders of magnitude improvement in temporal resolution compared with third-generation synchrotron sources. The remarkable stability of this first laser-driven soft-X-ray undulator source along with anticipated advances in laser-electron acceleration,[26,27] beam transport and undulator design hold promise for further progress: in the short term, we expect this approach to spawn laboratory-sized undulator radiation sources with ångstrøm wavelengths and sub-10-fs pulse durations for four-dimensional imaging with atomic resolution.[28] In the long term, these developments may culminate in the emergence of laboratory-scale ultra-brilliant X-ray free-electron lasers[29, 30] with revolutionary impacts on many fields of science, technology and medicine.

Methods

Simulation. Undulator radiation calculations are carried out with the code SRW (ref. 25). The effect of the magnetic lenses is taken into account using the Twiss parameters, determined by electron-beam optics with an initial electron source size of 2 μm and divergence of 1 mrad. The calculated near-field is subsequently propagated through the beamline, consisting of a spherical focusing mirror with a 10 m radius of curvature and a slit, onto the detector.

X-ray spectrometer. The spectrometer consists of a 1,000 lines mm^{-1} transmission grating with free-standing wires held by a support mesh. The radiation was detected by a Princeton Instruments SX-400 X-ray CCD (charge-coupled device) camera. Owing to a slight rotation of the grating with respect to the CCD camera, the parabolas drawn in Figure 3a are corrected accordingly. Stray light was blocked by a 700 μm slit in front of the grating. The wavelength calibration was deduced from plasma radiation, when the blocking foil (Figure 1) was removed, by the spectral cutoff through a 150 nm aluminum filter (17.1 nm) in front of the CCD. To deduce the number of photons emitted by the undulator, the wavelength-dependent reflectivity and efficiency of the gold mirror and the transmission grating as well as the wavelength-dependent quantum efficiency and conversion from CCD counts into detected photons have been taken into account.

Laser-plasma accelerator. The laser-wakefield accelerator is driven by the ATLAS Ti:sapphire laser system, which delivers pulses of 850 mJ energy on target with a 37 fs FWHM duration at a central wavelength of ~800 nm with a repetition rate of 10 Hz. The laser beam is focused by an f/22 off-axis parabola to a spot of 23 μm FWHM (corresponding to a normalized laser-vector potential of a_0=1.0) into a 15-mm-long hydrogen-filled gas cell of 200 μm diameter. At a plasma density of n_p=8 × 10^{18} cm^{-3}, electron bunches with an overall charge of 7 pC are injected into the laser wakefield and accelerated to energies of up to ~210 MeV (ref. 10). The average beam divergence after collimation with the magnetic lenses is 0.7 mrad with an r.m.s. angular shot-to-shot variation of 0.2 mrad.

Miniature magnetic quadrupole lenses and undulator.[11] The magnetic lenses with a field gradient of ~500 T m^{-1} over a radius of 3 mm are positioned ~25 cm after the accelerator in a doublet configuration with lengths of 17 mm and 15 mm, respectively. The permanent-magnet (NdFeB) undulator has a length of 30 cm with 5-mm-long periods constructed in a hybrid structure. At a gap of 1.2 mm between the magnetic poles, it has an undulator parameter of K = 0.55.

Acknowledgments — We thank M. Fieß, R. Ernstorfer, A. Cavalieri, E. Fill and M. Hofstetter for equipment. This work has been financially supported by the DFG through Transregio TR18 and supported by the DFG Cluster-of-Excellence "Munich-Centre for Advanced Photonics" MAP.

Author Contributions — M.F., R.W., A.P., Zs.M., S.B., J.O., S.K. and F.G. carried out the experiment. M.F., R.W., A.P., Z.M., S.B., J.O., R.H., G.T., U.S., T.P.R., S.M.H. and S.K. designed and fabricated the components of the experiment. M.F., I.C. and B.Z. analyzed the data. D.H., F.K., S.K. and F.G. provided overall guidance to the project.

References

1. Bilderback, D. H., Elleaume, P. & Weckert, E. Review of third and next generation synchrotron lightsources. J. Phys. B 38, 773–797 (2005).
2. Mangles, S. P. D. et al. Monoenergetic beams of relativistic electrons from intense laser plasma interactions. Nature 431, 535–538 (2004).
3. Geddes, C. G. R. et al. High quality electron beams from a laser wakefield accelerator using plasma-channel guiding. Nature 431, 538–541 (2004).
4. Faure, J. et al. A laser-plasma accelerator producing monoenergetic electron beams. Nature 431, 541–544 (2004).
5. Thomas, A. G. R. et al. Monoenergetic electronic beam production using dual collinear laser pulses. Phys. Rev. Lett 100, 255002 (2008).
6. Rowlands-Rees, T. P. et al. Laser-driven acceleration of electrons in a partially ionized plasma channel. Phys. Rev. Lett 100, 105005 (2008).
7. Faure, J. et al. Controlled injection and acceleration of electrons in plasma wakefields by colliding laser pulses. Nature 444, 737–739 (2006).
8. Leemans, W. P. et al. GeV electron beams from a centimetre-scale accelerator. Nature Phys. 2, 696–699 (2006).
9. Hafz, N. A. M. et al. Stable generation of GeV-class electron beams from self-guided laser-plasma channels. Nature Photon. 2, 571–577 (2008).
10. Osterhoff, J. et al. Generation of stable, low-divergence electron beams by laser wakefield acceleration in a steady-state-flow gas cell. Phys. Rev. Lett. 101, 085002 (2008).
11. Eichner, T. et al. Miniature magnetic devices for laser-based, table-top free-electron-lasers. Phys. Rev. ST Accel. Beams 10, 082401 (2007).
12. Schoenlein, R. W. et al. Generation of femtosecond pulses of synchrotron radiation. Science 287, 2237–2240 (2000).
13. Khan, S., Holldack, K., Kachel, T., Mitzner, R. & Quast, T. Femtosecond undulator radiation from sliced electron bunches. Phys. Rev. Lett. 97, 074801 (2006).
14. Gaffney, K. J. & Chapman, H. N. Imaging atomic structure and dynamics with ultrafast X-ray scattering. Science 316, 1444–1448 (2007).
15. Fritz, D. M. et al. Ultrafast bond softening in bismuth: Mapping a solid's interatomic potential with X-rays. Science 315, 633–636 (2007).
16. Barty, A. et al. Ultrafast single-shot diffraction imaging of nanoscale dynamics. Nature Photon. 2, 415–419 (2008).
17. Marchesini, S. et al. Massively parallel X-ray holography. Nature Photon. 2, 560–563 (2008).
18. Zholents, A. & Fawley, W. M. Proposal for intense attosecond radiation from an X-ray free-electron laser. Phys. Rev. Lett. 92, 224801 (2004).

19. Clarke, J. A. The Science and Technology of Undulators and Wigglers (Oxford Univ. Press, 2004).
20. Karsch, S. et al. GeV-scale electron acceleration in a gas-filled capillary discharge waveguide. New J. Phys. 9, 415 (2007).
21. Kameshima, T. et al. 0.56 GeV laser electron acceleration in ablative-capillary-discharge plasma channel. Appl. Phys. Express 1, 066001 (2008).
22. Matlis, N. H. et al. Snapshots of laser wakefields. Nature Phys. 2, 749–753 (2006).
23. Pukhov, A. & Meyer-ter-Vehn, J. Laser wake field acceleration: The highly non-linear broken-wave regime. Appl. Phys. B: Lasers Opt. 74, 355–361 (2002).
24. Schlenvoigt, H.-P. et al. A compact synchrotron radiation source driven by a laser-plasma wakefield accelerator. Nature Phys. 4, 130–133 (2008).
25. Chubar, O. & Elleaume, P. Accurate and efficient computation of synchrotron radiation in the near field region. Proc. EPAC98 1177–1179 (1998).
26. Geddes, C. G. R. et al. Plasma-density-gradient injection of low absolute-momentum-spread electron bunches. Phys. Rev. Lett. 100, 215004 (2008).
27. Malka, V. et al. Principles and applications of compact laser-plasma accelerators. Nature Phys. 4, 447–453 (2008).
28. Krausz, F. & Ivanov, M. Attosecond physics. Rev. Mod. Phys. 81, 163–234 (2009).
29. Nakajima, K. Compact X-ray sources: Towards a table-top free-electron laser. Nature Phys. 4, 92–93 (2008).
30. Grüner, F. et al. Design considerations for table-top, laser-based VUV and X-ray free electron lasers. Appl. Phys. B: Lasers Opt 86, 431–435 (2007).

Supplementary Information follows.

Supplementary Information to the manuscript "Laser-driven soft-X-ray undulator source"

Ultrashort electron bunch durations of laser-wakefield accelerators and elongation during beam transport

Although measurements of the pulse duration of laser-wakefield accelerated electron bunches[1] have not yet been conducted with sufficient temporal resolution, theory and simulations[2] suggest durations on the order of the plasma wavelength, which is in our case ~15 μm. Moreover, the observation of electron energy spectra with a quasi-mono-energetic peak indicates that the electron bunch occupies only a fraction of the wakefield's accelerating phases. Therefore, the bunch duration at the exit of the laser-plasma accelerator in the bubble regime[2] is a fraction of the plasma period – as confirmed by PIC simulations, which indicates durations on the order of 10 fs (FWHM).

Since the undulator is positioned ~50 cm after the exit of the accelerator, the influence of degrading effects that elongate the bunch duration during beam transport, such as space-charge effects, path-length differences due to angular spread and chromatic effects of the lenses as well as energy spread have to be taken into account. Supplementary Figure 1 shows the bunch-duration evolution of a 10 fs long electron bunch along our setup simulated by a tracking algorithm[3], which includes all degrading effects mentioned above. According to this simulation, a bunch with a longitudinal RMS-length of 2.95 μm (9.8 fs) elongates to 3.06 μm (10.2 fs) over the distance of our beamline, which extends from the exit of the accelerator to the exit of the undulator (at ~0.8 m) and includes the magnetic lenses.

In our case, the predominant effect in the growth of bunch duration is the path length difference due to a finite emittance electron beam, i.e. the path-length difference of an electron with a finite divergence in comparison to a zero-divergence electron. In the case of a free drift (no magnetic lenses, green curve in Supplementary Fig. 1), the path

difference grows perpetually along the whole setup. For our beamline with lenses (red curve in Supplementary Fig. 1), the path difference increases similar to the free drift

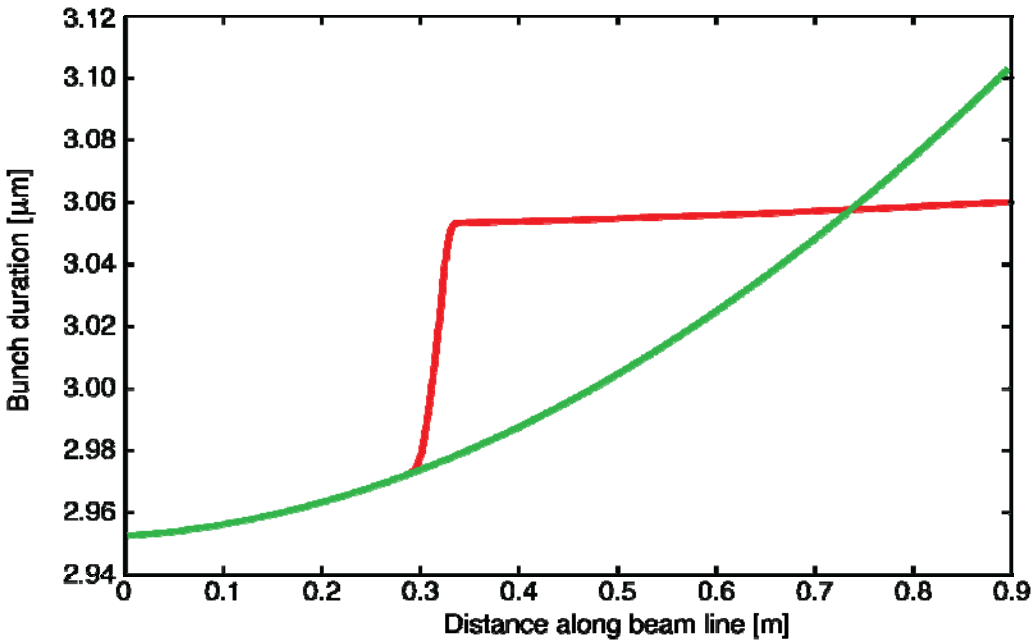

Supplementary Figure S1| Simulation of the evolution of the electron bunch duration along the beamline. The red curve shows the bunch-duration evolution of an electron bunch that is propagating through the beamline including the magnetic lenses, (which are positioned at 28 cm and 32 cm; the undulator at 50-80 cm), and the green curve shows the growth of the duration of a free-drifting bunch. Both curves are simulated with a tracking code[3] with an initial bunch duration of 10 fs, an initial RMS-divergence of 1 mrad and RMS-source size of 2 μm, a charge of 5 pC and an energy of 210 MeV with an RMS-energy spread of 3.5%.

until the bunch reaches the first lens, then it grows rapidly, since the first lens is defocusing in the horizontal direction. After the second lens (which is horizontally focusing) the electron beam is collimated (see the yellow envelope in main text Fig. 2a) and therefore no more path length difference is accumulated, which means that the bunch duration remains almost constant. An analytical beam-transport calculation of an electron with an initial divergence of 1mrad (one standard deviation of the divergence

distribution) and a zero-divergence electron, both propagating through the lens setup, leads to a path-length difference of ~0.5 μm (~2.4 fs). A convolution with the whole temporal Gaussian bunch distribution of 10fs RMS gives an increase in bunch duration of 0.3 fs, which agrees very well with the simulated results.

The elongation of the bunch duration due to electron-energy spread and the resulting time of arrival differences for electrons with different energies can be neglected in our case. The simulated durations for a bunch without energy spread does not significantly differ from a bunch with an RMS energy-spread of 3.5% (corresponding to the width of the *effective* electron spectrum). An analytical upper limit for two zero-emittance electrons with energies of 200 and 210 MeV, respectively, yields an arrival-time difference of 0.8 fs. Simulations for a bunch with a charge of 5 pC show that space-charge effects also do not have a significant influence on the duration. Space-charge primarily leads to the development of an energy chirp along the bunch hence increase the initial energy spread[4] as well as increase the initial beam divergence due to Coulomb explosion. Yet, for the relatively small charge of 5 pC, the transverse bunch expansion is mainly driven by the initial divergence.

Tunability of undulator radiation

By changing the distances of the magnetic quadrupole lenses, different electron energies can be focussed at the position of the detector, which can be used to shift the system response function (main text Fig. 2b). Supplementary Fig. 2 shows the system response curve for three different lens settings. The different peak energies of the curves show that the source can be tuned over a wide range of wavelengths with this method. The narrow bandwidths of the curves are a result of the electron-energy dependent divergence effects induced by the chromaticity of the magnetic lenses (as discussed in the main text), which depend only very weakly on the peak energy of the system response function.

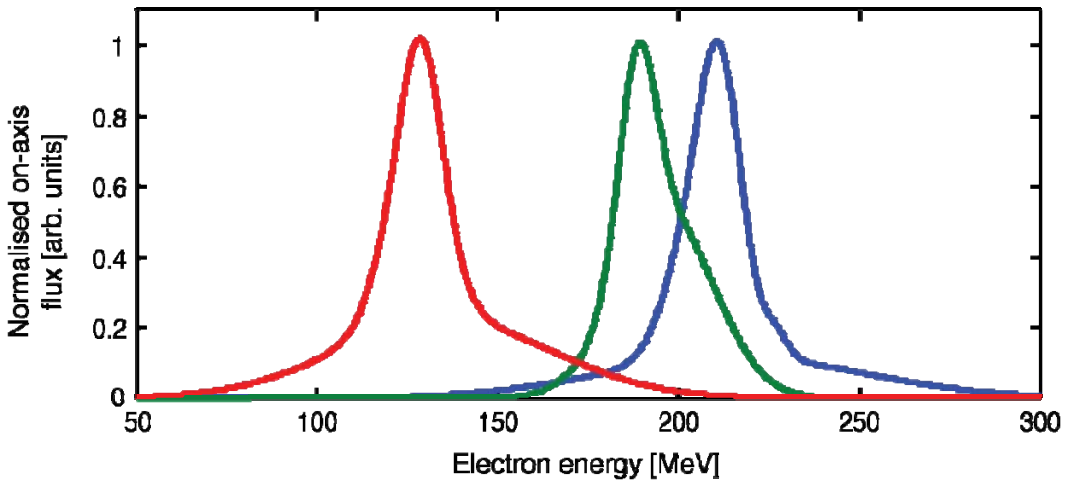

Supplementary Figure S2| Simulated on-axis undulator flux. The normalised on-axis undulator flux (system response function) is simulated for three different lens settings. The blue and the green curves are the respective response functions for the lens settings used to measure the blue and green data points in main text Fig. 4. The red curve demonstrates the wide range of wavelength-tunability.

References

1. van Tilborg, J. *et al.* Terahertz radiation as a bunch diagnostic for laser-wakefield-accelerated electron bunches. *Phys. Plasmas* **13**, 056704 (2006).

2. Pukhov, A. & Meyer-ter-Vehn, J. Laser wake field acceleration: the highly non-linear broken-wave regime. *Appl. Phys. B: Lasers Opt.* **74**, 355–361 (2002).

3. Pulsar physics and the general particle tracer (GPT) code. http://www.pulsar.nl/gpt (2009).

4. Grüner, F., Schroeder, C.B., Maier, A.R., Becker, S. & Mikhailova, Y.M. Space-charge effects in ultra-high current electron bunches generated by laser-plasma accelerators. *Phys. Rev. ST Accel. Beams* **12**, 020701 (2009).